Surface plasmon resonance imaging reveals multiple binding modes of Agrobacterium transformation mediator VirE2 to ssDNA

Sanghyun Kim, David Zbaida, Michael Elbaum, Hervé Leh, Claude Nogues, Malcolm Buckle

Nucleic Acids Research Advance Access published June 4, 2015

doi: 10.1093/nar/gkv571

Surface plasmon resonance imaging reveals multiple binding modes of Agrobacterium transformation mediator VirE2 to ssDNA

Sanghyun Kim[1], David Zbaida[1], Michael Elbaum[1,*], Hervé Leh[2], Claude Nogues[2] and Malcolm Buckle[2,*]

[1]Dept of Materials and Interfaces, Weizmann Institute of Science, 7610001 Rehovot, Israel and [2]LBPA, Institut d'Alembert, ENS de Cachan, CNRS, 61, avenue du Président Wilson, F-94235 Cachan, France

Received December 09, 2014; Revised March 19, 2015; Accepted May 20, 2015

ABSTRACT

VirE2 is the major secreted protein of *Agrobacterium tumefaciens* in its genetic transformation of plant hosts. It is co-expressed with a small acidic chaperone VirE1, which prevents VirE2 oligomerization. After secretion into the host cell, VirE2 serves functions similar to a viral capsid in protecting the single-stranded transferred DNA en route to the nucleus. Binding of VirE2 to ssDNA is strongly cooperative and depends moreover on protein–protein interactions. In order to isolate the protein–DNA interactions, imaging surface plasmon resonance (SPRi) studies were conducted using surface-immobilized DNA substrates of length comparable to the protein-binding footprint. Binding curves revealed an important influence of substrate rigidity with a notable preference for poly-T sequences and absence of binding to both poly-A and double-stranded DNA fragments. Dissociation at high salt concentration confirmed the electrostatic nature of the interaction. VirE1–VirE2 heterodimers also bound to ssDNA, though by a different mechanism that was insensitive to high salt. Neither VirE2 nor VirE1–VirE2 followed the Langmuir isotherm expected for reversible monomeric binding. The differences reflect the cooperative self-interactions of VirE2 that are suppressed by VirE1.

INTRODUCTION

Agrobacterium tumefaciens is a common, Gram negative soil bacterium with a unique capability for inter-kingdom gene transfer (1,2). In nature the transgene products cause the 'crown gall' disease, which leads to neoplastic growths or tumors on plant stems and synthesis of opine compounds by infected tissues. Agrobacterium uses these compounds as carbon and nitrogen sources, providing it a competitive advantage. In the laboratory the transfer DNA may be replaced by any sequence of interest, making this organism a powerful vector for synthetic genome modification (3).

Most of the machinery for pathogenesis resides on a long tumor-inducing plasmid (Ti-plasmid), including regions encoding for virulence protein expression and opine catabolysis, as well as the transfer DNA (T-DNA) itself. Transfer of both DNA and disease effector proteins involves a type IV secretion system akin to that involved in conventional bacterial conjugation (4,5). Also in analogy to conjugation, the T-DNA is delivered as a single-stranded linear oligonucleotide, the T-strand, with a mobility protein (VirD2) bound covalently at the 5′ end. However, as the target is a plant, the cytoplasmic environment of the recipient cell is very different from that of the donor.

VirE2 is a large, single-stranded DNA binding protein that serves to protect the T-strand from cytoplasmic nucleases and to adapt it for nuclear import (6–8). VirE2 is expressed together with VirE1, a small secretion chaperone that maintains VirE2 in soluble form as a heterodimer (9,10). Thus VirE2 may be regarded as a secreted disease effector, as a capsid protein, or as an adapter of bacterial conjugation to a eukaryotic host.

The T-strand and VirE2 are the most essential components in the infection process, yet they need not originate from the same bacterium. This has led to the conclusion that the two may be secreted individually and meet only in the host cytoplasm (11,12). Another indication comes from a chromatin immunoprecipitation-like 'TrIP' assay, in which immunoprecipitates of specific virulence proteins from activated bacteria were assayed by polymerase chain reaction for the presence of T-strand. No direct interaction between VirE2 and T-strand was detected (13). On the other hand, upon virulence activation VirE2 becomes the most abundant single protein in Agrobacterium (14,15). Therefore the

*To whom correspondence should be addressed. Tel: +972 8 9343537; Fax: +972 8 9344138; Email: michael.elbaum@weizmann.ac.il
Correspondence may also be addressed to Malcolm Buckle. Tel: +33 1 47407673; Fax: +33 1 47407671; Email: buckle@lbpa.ens-cachan.fr
Present Address: Sanghyun Kim, Dep. of Bio and Brain Engineering, KAIST, Daejeon, 305-701, Republic of Korea.

molecular binding of VirE2 to ssDNA both in the presence and the absence of VirE1 are important for understanding the infection mechanism of *Agrobacterium tumefaciens,* as these represent conditions in the bacterium and in the plant, respectively.

In vitro, VirE2 binds ssDNA cooperatively to form a solenoidal protein shell surrounding the oligonucleotide. This is believed to represent the relevant form *in planta*. Structural parameters of this T-complex have been determined by quantitative STEM imaging (16) and by three-dimensional reconstruction from TEM images (17,18). Two binding modes have been observed with similar pitch but different diameters of approximately 13 and 16 nm. These contain 3.3 or 4.3 protein units per turn, respectively, and are estimated to accommodate a footprint of 16–19 nucleotide bases each. A high-resolution structure of VirE2 in complex with VirE1 was also determined by X-ray diffraction (19). This analysis showed two very similar central domains joined by a flexible linker in between. The first 111 amino acids were missing in this analysis, as were the terminal 39 amino acids that correspond to an arginine-rich secretion signal (20). [These studies were performed using the nopaline strain VirE2; the octopine strain differs mainly by truncation of 23 amino acids at the unfolded N terminus.] A recent application of advanced hybrid methods, including three-dimensional cryo-EM, computational modelling, chemical modifications, electron paramagnetic resonance spectroscopy and mass spectroscopy, enabled the docking of the N-terminal central domain within the EM envelope and revealed the architectural plan of the complex that provides a rigid structure overall while maintaining local flexibility (18). Longitudinal or 'ring to ring' protein contacts along the solenoid axis are made between N terminal domains of a given protein and its third (or fourth) neighbor around the circumference. This provides a structural mechanism for cooperativity in binding ssDNA.

VirE2 over-expressed in *E. coli* (without VirE1) goes into insoluble inclusion bodies from which it must be extracted by denaturation and refolding. Moreover it precipitates above a concentration of 0.25–0.5 mg/ml, depending on the ionic strength of the buffer. Gel filtration shows that the protein is found in large oligomers even at such low concentrations; when imaged by TEM the protein is found in long filamentous aggregates (10). Their outer diameter is close to that of the DNA complex, so although disordered, their local structure is probably similar to that of the assembled T-complex. When mixed with ssDNA, these filamentous aggregates are converted into the ordered complex. Most strikingly, the conversion does not involve a re-polymerization along the DNA substrate, but rather a conversion of the local protein organization. This is most clearly seen by assembly on short DNA oligomers comparable in length to the single protein-binding footprint. The same ordered structure is observed as on long ssDNA substrates (10,17,18).

The binding interface to VirE1 lies in between the central domains and clamps the two domains together in a 'closed' conformation that prevents oligomerization from the ends (19). Thus VirE1–VirE2 is a soluble heterodimer; this is most likely the primary function of VirE1 as a secretion chaperone, to keep VirE2 in an export-competent state. Although VirE1 is strongly acidic and the structural data identifies electrostatic contacts to a positively charged face of VirE2, the heterodimer remains stable at high salt (9). This might reflect interactions between amino acids not seen in the crystal structure, suggesting more than a single mode of binding.

VirE1–VirE2 interacts rapidly with ssDNA (21). Upon binding to long ssDNA this entails a release of VirE1 (10,21), but very short (26 or 32-mer) oligonucleotides do not disrupt the VirE1–VirE2 interaction (9,10). A partial reversibility is observed in the interaction of VirE2 (from VirE1–VirE2) with 170-mer ssDNA (21). In the case of VirE2 alone, binding stoichiometry is shifted for short oligonucleotides, consistent with a reduced cooperativity in comparison to long ssDNA (10). Notably, chemical modification of VirE2 at the longitudinal interface one turn around the solenoid interrupts DNA binding (18). This represents a sort of hyper-allostery in which the quaternary form of the protein is required for its interaction with the DNA ligand.

In this work we explore the binding of VirE2 to ssDNA substrates with real time kinetics, with an emphasis on direct interaction and sensitivity to local rigidity. These parameters are difficult to isolate in solution assays due to the tendency to form long DNA-protein complexes even from short oligonucleotides. Therefore we took an approach to immobilize short ssDNA substrates on a surface and to detect the protein interaction by surface plasmon resonance (SPR) imaging. SPR is a optical effect sensitive to mass adsorbed to a liquid-exposed surface. It has been widely applied to the study biomolecular interactions, and is closely associated with quantification of binding constants in a controlled environment with low non-specific binding. The imaging variant (SPRi) provides directly resolved access to the measured surface reflectivity from which the adsorbed quantities can be extracted (22,23).

Neither the binding of VirE2 nor of VirE1–VirE2 to ssDNA conformed to a classic Langmuir isotherm based on equilibrium mass action kinetics. This precluded a standard thermodynamic analysis in the tradition of SPR. Nevertheless, comparison between the two protein forms and their interaction with different DNA substrates was very informative. VirE2 has a strong tendency to oligomerize in solution, consequences of which could be recognized in the surface binding. VirE2 binding to poly-A or poly-T sequences was dramatically different; this is consistent with differences in the local rigidity of the DNA due to base stacking. VirE1–VirE2 complexes were also found to interact with surface-bound ssDNA and to distinguish poly-A from poly-T. Unlike VirE2, the binding of VirE1–VirE2 to ssDNA was stable in a high salt buffer, indicating a distinct mode of interaction with the oligonucleotide.

MATERIALS AND METHODS

Protein purification

VirE2 was expressed and purified from inclusion bodies according to our published procedure (10) with modifications in the purification step. Specifically, the *virE2* gene (nopaline strain, protein accession number P08062) was cloned into the pET-28b vector (Novagen) and expressed in E. coli

BL21(DE3) strain by induction with 1 mM IPTG at 37°C for 3 h. Following sonication in buffer A (10 mM Hepes 7.4, 100 mM NaCl, 1 mM EDTA, 1 mM DTT and 10% glycerol) including 1 mM PMSF (Sigma) and 170 units of protease inhibitor cocktail (CalBiochem), inclusion bodies were isolated by washing in buffer A with 2% Triton X-100 three times and then washed in buffer B (20 mM Hepes 7.4, 1 M NaCl, 1 mM EDTA) and denatured in 5 M Urea in buffer A. Following refolding by dialysis against buffer C (10 mM KH_2PO_4 pH 7.4, 0.1 mM $CaCl_2$, 1 mM DTT), VirE2 was captured on a heparin column (Pharmacia HiTrap heparin) using Tris buffer 50 mM, pH 8, and eluted with a gradient up to 1 M NaCl. Purified fractions of the protein were collected at NaCl concentration of 450–600 mM. Glycerol (10% V/V) and DTT (1 mM, final concentration) were added for storage. Final protein concentrations ranging from 0.1 mg/ml to 1 mg/ml were measured by absorbance at 280 nm and by Bradford assay. Protein fractions were pooled separately and stored at -80°C.

As detailed in Ref (10), *virE1* ((P08063)) and *virE2* genes were cloned into pACYCDuet-1 (Novagen). VirE1 bears an N-terminal His_6 tag followed by a TEV cleavage site (ENLYFQG), whereas VirE2 is untagged. BL21(DE3) cells harboring the VirE1–VirE2-duet plasmid were induced by 0.05 mM IPTG at OD600 0.6. The culture was harvested after additional growth for 18 h at 15°C. Bacterial pellets were sonicated in buffer B (as above). The VirE1–VirE2 complex was captured on a Ni-chelating column (Pharmacia HiTrap-Chelating) and eluted at 200 mM imidazole. Following buffer exchange by dialysis to buffer C, the complex was purified on a Heparin column (Pharmacia HiTrap Heparin), with 1 M NaCl. The VirE1–VirE2 complex eluted at 200 mM NaCl and was treated with TEV protease to remove the His tag from VirE1. Final purification of the complex was made by gel filtration in 50 mM Tris pH 8.0 with 150 mM NaCl, 1 mM DTT, 1 mM EDTA.

Concentration of VirE2 and of VirE1–VirE2 differed drastically. Due to the low solubility of VirE2 and its tendency to high-order oligomeric form even in solution (10), the most concentrated solution used for kinetic studies involved a dilution 1/20 from a 0.3 mg/ml stock, corresponding to 4.5 μM. At stock dilutions greater than 1/200 the signal from surface adsorption became immeasurably small. The VirE1–VirE2 heterodimer is highly soluble, on the other hand. The stock solution concentration was 6.4 mg/ml and accessible experimental concentrations ranged up to 90 μM.

DNA fragments

40-mer poly-T and poly-A sequences with a 5′ C6-thiol modifier, as well as unmodified oligonucleotides were from MWG-Eurofins (France). 5′ thiol and internal C3 spacer-modified oligonucleotides were from Sigma-Proligo (France). Random primer sequences were derived from pGEMT easy vector positions 619–638, 619–641, 617–659 and 617–666 for 20, 23, 43 and 50 mer respectively. (Unmodified, reverse-complement sequences were used for production of dsDNA, i.e., 638–619, 641–619, etc.) Sequences are shown below.

Mi20C3

HS-(CH2)6-TTTTT-(CH2)6-CGACGCTCAAGTCAGAGGTG

MI20C

CACCTCTGACTTGAGCGTCG

Mi23C3

HS-(CH2)6-TTTTT-(CH2)6-CGACGCTCAAGTCAGAGGTGGCC

MI23C

GGCCACCTCTGACTTGAGCGTCG

MI43C3

HS-(CH2)6-TTTTT-(CH2)6-ATCGACGCTCAAGTCAGAGGTGGCCAAACCCGACAGGACTATA

Mi43C

TATAGTCCTGTCGGGTTTCGCCACCTCTGACTTGAGCGTCGAT

MI50C3

HS-(CH2)6-TTTTT-(CH2)6-ATCGACGCTCAAGTCAGAGGTGGCGAAACCCGACAGGACTATAAAGATAC

MI50C

GTATCTTTATAGTCCTGTCGGGTTTCGCCACCTCTGACTTGAGCGTCGAT

In order to produce double-stranded DNA binding fragments, modified oligonucleotides were mixed with an excess of the complementary non-thiolated ssDNA to ensure that all thiolated DNA were double stranded to a final concentration of 10 μM in 100 mM NaCl. After heating at 95°C for 5 min, hybridization was effected by slow cooling.

SPR measurement

The technique of DNA immobilization was applied essentially as described (23). DNA surfaces were prepared on a high-refractive index glass prism (type SF 10: n 1.707987 at $\lambda = 830$ nm) activated by Reactive Ion Etching (RIE) prior to the thermal evaporation of a 50 nm gold layer. First, a fresh gold layer was immersed in a solution containing 0.1 mM of 1-undecanethiol substituted with a hydroxyl-terminated tetra(ethylene glycol) (EG_4-OH) diluted in ethanol for 30 s at room temperature. Before DNA deposition the prisms were thoroughly rinsed in pure ethanol twice for 20 min. The DNA solution (3 or 5 μM starting concentration) was spotted on the freshly pretreated prism surface in phosphate buffer (0.4 M) at pH 7.4 and incubated for 16 h in a sealed Petri dish at 100% relative humidity to prevent the DNA solution from drying. Moreover, in order to reduce evaporation during incubation, the DNA solution contained 5% glycerol. The prism was then directly inserted into the SPRi apparatus (GenOptics, France) and buffer (50 mM Tris pH 8.0 with 100mM NaCl) was immediately flowed across the surface at 25 μl/min. To remove any excess of DNA or unbound DNA from the surface, 200 μl of sodium dodecyl sulphate (SDS) diluted to 0.1% (w/v) was injected across the surface at 25 μl/min, followed by another wash with loading buffer.

For binding assays the protein stock solutions were diluted directly into SPRi loading buffer: 50 mM Tris pH 8.0 with 100 mM NaCl or higher as indicated and flowed across the prism surface at 12.5 μl/min. Reflectivities were recorded from an array of DNA spots in association phase, and then in dissociation upon switching to flow of protein-

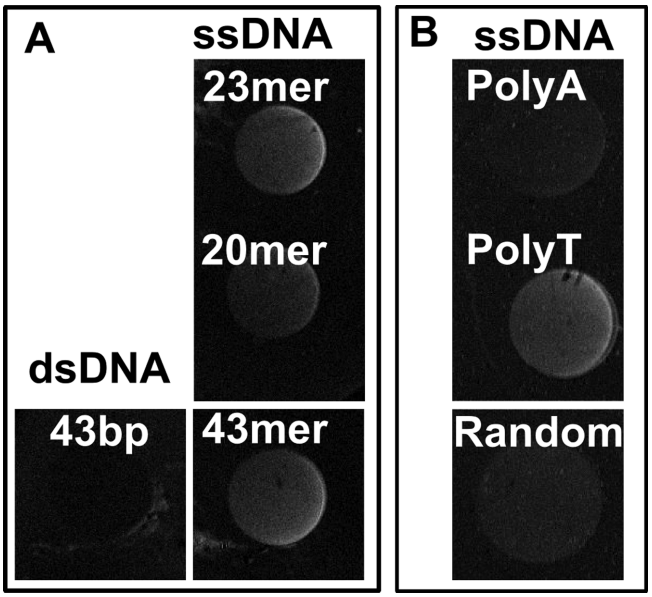

Figure 1. SPRi images testing association of VirE2 to DNA substrates as marked: (**A**) dsDNA 43 bp, ssDNA 20-, 23- or 43-mer random sequences at 470 nM protein concentration, (**B**) 40-mer poly-A, poly-T and 50-mer random sequences at 94 nM protein concentration.

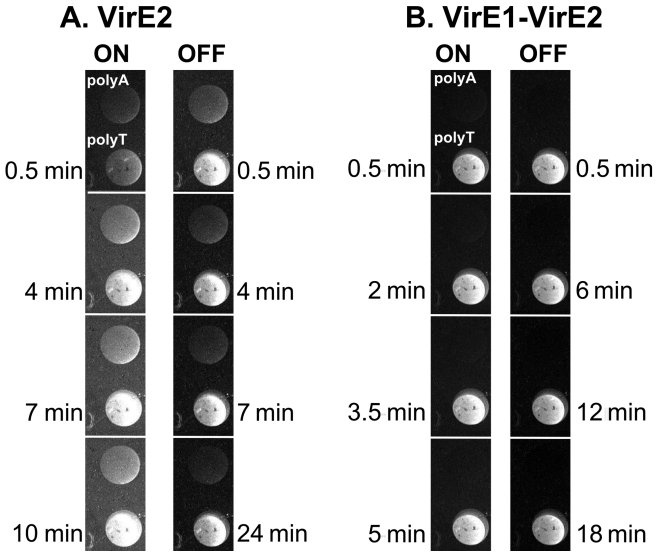

Figure 2. SPRi images of binding and dissociation on 40-mer poly-A and poly-T ssDNA substrates. (**A**) VirE2 at 94 nM concentration, (**B**) VirE1–VirE2 at 453 nM concentration. Times marked indicate the duration from the start of the injection of protein (ON) and from the exchange with protein-free buffer (OFF).

free buffer. The surface was regenerated with SDS 0.1% as described above followed by washing with buffer. For high salt assays the Tris concentration was maintained at 50 mM while NaCl was increased.

Electron microscopy

DNA-protein complexes were deposited on freshly glow-discharged carbon-coated grids, stained with 1.5% uranyl acetate solution and air-dried. Images were recorded to CCD camera in a transmission electron microscope (FEI Tecnai T12 Spirit).

RESULTS AND DISCUSSION

Binding of VirE2 and VirE1–VirE2 to immobilized DNA fragments

VirE2 normally binds cooperatively to long ssDNA substrates. In order to limit the interaction to the scale of the binding footprint we worked with short surface-immobilized oligonucleotides. We first established that VirE2 in fact binds to these short substrates. DNA fragments were spotted onto the SPRi sample surface as described in Materials and Methods and washed with the loading buffer. Purified VirE2 protein was then flowed across the surface. Figure 1A shows differential images during the association period as the VirE2 protein interacts with separate spots containing DNA constructs matching roughly one and two protein binding footprints. In accordance with earlier observations in bulk solution where VirE2 shows no affinity to dsDNA (24) no binding to dsDNA is detected, but images confirm binding to 20-, 23- and 43-mer ssDNA substrates (Figure 1A). The observations are consistent with the structural model based on electron microscopy, wherein ssDNA is wrapped around the inner circumference of a solenoidal shell. The inner radius of curvature is approximately 3 nm, which is comparable to the persistence length of ssDNA and much smaller than that of dsDNA. Thus we expect that short ssDNA fragments may interact with the same binding face as long ssDNA in a mature complex, while this is not possible for dsDNA. We found results on 40–50 base lengths to be more consistent than 20-mer, most likely due to steric interference from the surface. Therefore we continued with the slightly longer oligomers. We then addressed the possibility of a sequence-rigidity dependence of VirE2 binding to short DNA segments. Purine base stacking causes poly-A to adopt a more rigid structure than poly-T or mixed sequences (25). In order to test for an effect, the experiment was repeated with 40-mer poly-A and poly-T (Figure 1B).

Kinetic changes in the reflectivity signals are shown in Figure 2 for poly-A and poly-T bound spots as VirE2 or VirE1–VirE2 protein was flowed across the surfaces, and as it was removed by buffer flow. VirE2 bound most strongly to poly-T, the most flexible of the tested substrates. Weak binding to poly-A is seen clearly for both VirE2 and VirE1–VirE2; for the latter it is undetectable while poly-T binding appears strong. Note the very slow dissociation of both proteins from poly-T, indicating an important contribution of substrate flexibility.

The very different binding of VirE2 to poly-A and poly-T substrates was confirmed by electron microscopy. Figure 3 shows a representative field in which extended solenoids (arrows) are abundant in the poly-T case. Well-formed solenoidal complexes on poly-A ssDNA were rare. In the background we observed what appears to be small protein aggregates (arrowheads).

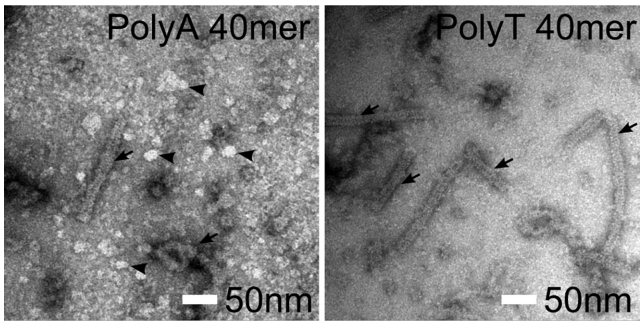

Figure 3. Representative images of VirE2-ssDNA complexes formed on 40-mer poly-A and poly-T substrates, visualized by transmission electron microscopy.

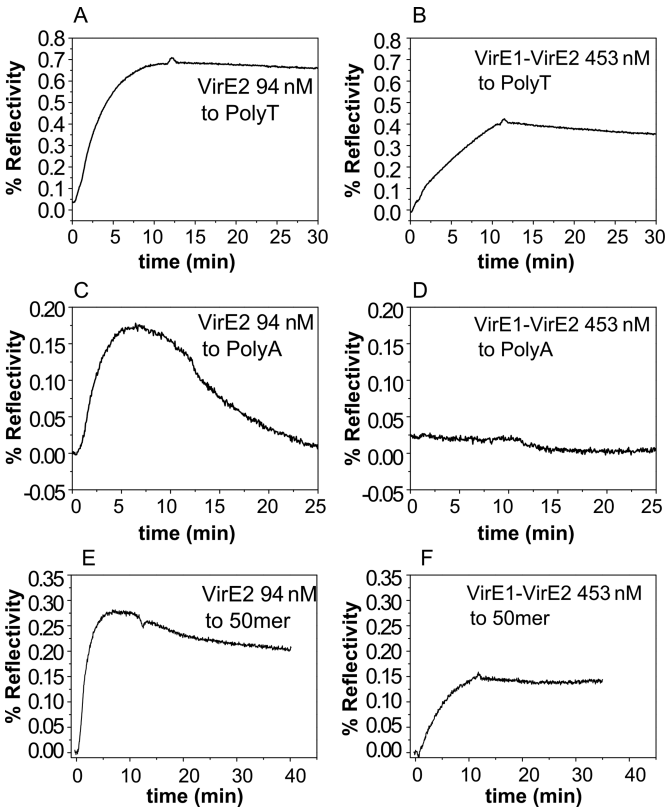

Figure 4. SPRi derived binding curves showing changes in % reflectivity as a function of VirE2 (94 nM) and VirE1–VirE2 (453 nM) binding to immobilized (**A**, **B**) poly-T, (**C**, **D**) poly-A or (**E**, **F**) random 50-mer on an SPRi surface.

Binding kinetics reveal distinct modes of interaction

Kinetic data of the type shown in Figure 4 were fit to exponential curves in order to obtain formal rate constants. Results appear in Table 1. The motivation for the fit was a simple Langmuir binding model, which, however, turned out to be inconsistent with the observations. Hence the fit parameters are useful for comparison of different DNA substrates but their biophysical implications must not be over-interpreted. The apparent dissociation rate constant k_{off} is obtained by fitting the dissociation phase to a simple exponential expression where the relative change in % reflectivity (R) as a function of time (t) with respect to R at time t = 0, (R_0), results from $R_t = R_0 \exp^{(-k_{\mathrm{off}}t)}$. The apparent association rate constant k_{on} is obtained from the fit to $R_t = R_{\mathrm{max}}(1 - \exp^{-(k_{\mathrm{on}}[C]+k_{\mathrm{off}})t})$ at a given protein concentration [C], where R_{max} is the response at steady state. According to the Langmuir paradigm the calculated equilibrium affinity K_d is simply the ratio $\frac{k_{\mathrm{off}}}{k_{\mathrm{on}}}$, from which we obtain values on the order of 1–10 nM. As we will see in the following, however, the binding cannot be interpreted in the context of a simple mass action paradigm of partitioning between bound and unbound states. Nonetheless we can understand '$k_{\mathrm{on}}[C]$' and 'k_{off}' phenomenologically as rates for binding and dissociation respectively, e.g. while smaller $k_{\mathrm{on}}[C]$ means a slower binding, smaller k_{off} indicates a longer time for dissociation. Note that the comparison is made for solution concentrations of VirE2 and VirE1–VirE2 that yield similar SPR reflectivities on the order of 1%, implying comparable net protein adsorption. (We present $k_{\mathrm{on}}[C]$ as the numerical fit parameter. Extraction of a true kinetic constant k_{on} would require measurement over a range of concentration and is predicated on thermodynamic assumptions that were not met.) In comparing between different ssDNA substrates, VirE1–VirE2 in general showed slower kinetics than VirE2 for both association and dissociation. In particular the dissociation of VirE1–VirE2 from ssDNA was negligible on the accessible time scale. By contrast, poly-A association was too weak even to fit. In the following we focus on the difference between VirE2 and VirE1–VirE2 binding to poly-T.

Figure 5A and B shows association and dissociation curves for VirE2 and VirE1–VirE2 complexes with 40-mer poly-T ssDNA substrates as a function of protein concentration. The range of accessible concentrations for VirE2 is much smaller due to its limited solubility. On the other hand, throughout the concentration range accessible to both proteins, quantitatively more VirE2 bound to the ssDNA than did VirE1–VirE2. Figure 5C shows a plot of the steady state signal versus solution concentration in each case, again with a striking difference. Simple equilibrium partitioning between bound and solution phases should produce a Langmuir isotherm. Instead, for the VirE2 we see an association increasing linearly from zero in proportion to the solution concentration, and for the VirE1–VirE2 we see what appears to be a Brunauer–Emmett–Teller (BET) type isotherm with a long plateau and sudden increase in binding at high concentration. This suggests that VirE1–VirE2 binds monomerically up to initial saturation, but then at high solution concentration recruits additional monomers by condensation to the resulting nucleoprotein complex. Neither binding mode for VirE2 nor VirE1–VirE2 is consistent with simple mass action equilibrium between monomeric bound and solution phases.

Notwithstanding the complexity of the interactions, VirE1–VirE2 appears to bind ssDNA by a different mechanism than VirE2. Following the BET paradigm we take the plateau in the VirE1–VirE2 signal as a measure of single-layer coverage without higher-order structures. This implies that binding of VirE2 (without VirE1) at very moderate concentration exceeds the stoichiometric capacity of the surface-bound ssDNA. Our interpretation is that aggre-

Table 1. Phenomenological kinetic parameters for binding of VirE2 (94nM) or of VirE1–VirE2 (453nM) to ssDNA substrates

	VirE2 (94nM)		VirE1–VirE2 (453nM)	
DNA	k_{off} s^{-1}	k_{on} $M^{-1}s^{-1}$	k_{off} s^{-1}	k_{on} $M^{-1}s^{-1}$
ss20	$4.09 \cdot 10^{-4}$	$3.34 \cdot 10^{4}$	$2.39 \cdot 10^{-5}$	$1.71 \cdot 10^{4}$
ss23	$3.55 \cdot 10^{-4}$	$4.49 \cdot 10^{4}$	$3.13 \cdot 10^{-5}$	$1.60 \cdot 10^{4}$
ss43	$5.19 \cdot 10^{-4}$	$5.53 \cdot 10^{4}$	$3.79 \cdot 10^{-5}$	$1.21 \cdot 10^{4}$
ss50	$1.53 \cdot 10^{-4}$	$12.44 \cdot 10^{4}$	$4.04 \cdot 10^{-5}$	$1.23 \cdot 10^{4}$
ssT40	$0.61 \cdot 10^{-4}$	$6.04 \cdot 10^{4}$	$8.29 \cdot 10^{-5}$	$3.30 \cdot 10^{3}$

As described in the text these raw fitting parameters are most useful for comparison among substrates for a given protein form, or between VirE2 and VirE1–VirE2 for the same DNA substrate. (Binding of VirE1–VirE2 to 40-mer poly-A substrates was too weak to fit clearly to the exponential form.) The numerical values should not be over-interpreted according to a conventional Langmuir binding paradigm which is not consistent with the underlying mechanism.

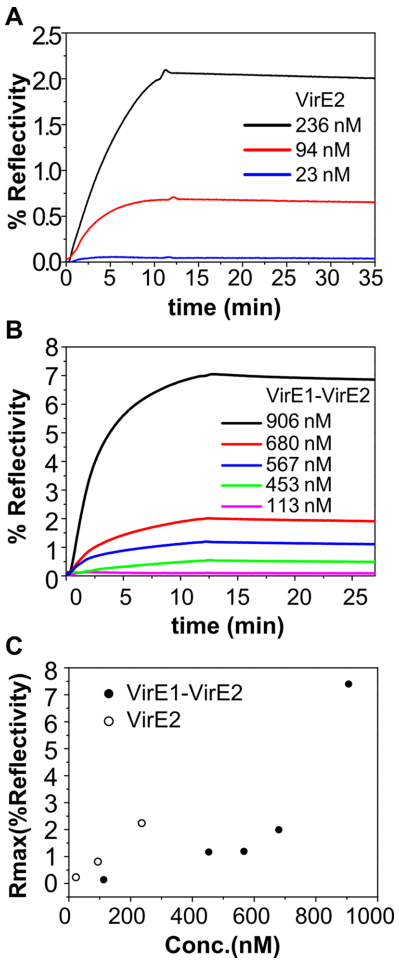

Figure 5. SPRi derived binding curves to 40-mer poly-T immobilized on an SPRi surface for (**A**) VirE2 and (**B**) VirE1–VirE2, with concentrations as marked. (**C**) Plot of the estimated asymptote (R_{max}) for binding of VirE2 and VirE1–VirE2 to poly-T. R_{max} was calculated from the curves shown in (a, b) using the simple expression $R_t = R_{max}\left(1 - \exp^{-(k_{on}[C]+k_{off})t)}\right)$ as explained in the text.

gates of VirE2 protein already present in solution bind to the surface at discrete points. These aggregates lie within the sensitivity depth of the surface plasmon resonance. Their characteristic size, and therefore the strength of the SPR signal, depends on the VirE2 concentration.

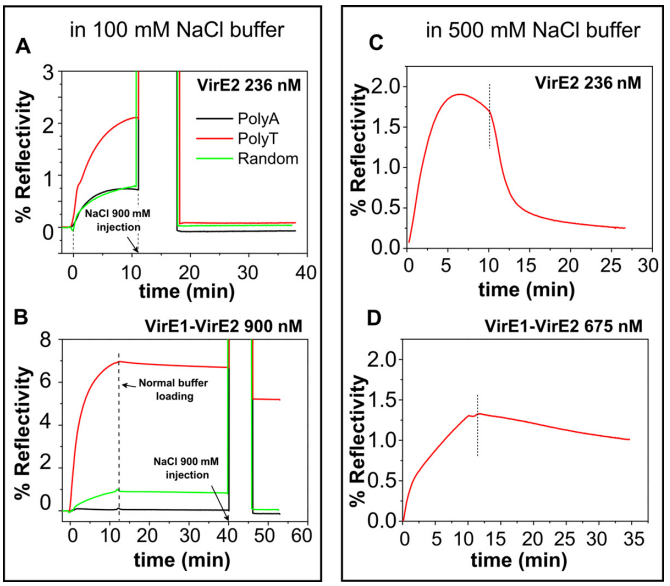

Figure 6. SPRi binding and dissociation curves including effects of high salt. (**A**) VirE2 at the highest accessible concentration of 236 nM on poly-A, poly-T and random sequence substrates as marked. (**B**) VirE1–VirE2 binds strongly to poly-T and weakly to random 50 mer; no binding is detected to poly-A (colors as in panel A). Dissociation is incomplete both with normal loading buffer (100 mM NaCl) and with high salt buffer (at 40 min, 900 mM NaCl injection). (**C**) VirE2 binding and dissociation in 500 mM NaCl buffer. Note the rapid dissociation, in contrast to the case at 100 mM NaCl—compare Figure 4A. (**D**) VirE1–VirE2 binding and dissociation in 500 mM NaCl buffer. In this case dissociation remains slow, consistent with incomplete dissociation at 100 mM NaCl (Figure 4B).

Effect of ionic strength on interaction with ssDNA

We next tested whether a high salt buffer solution would disrupt the stable complex of ssDNA and VirE2 (Figure 6). Association was conducted as normal at 100 mM NaCl, and then the high salt buffer (900 mM NaCl) was injected (Figure 6A). As seen, the protein adsorbed most strongly to the poly-T substrate and came off rapidly in the high salt buffer. In the case of VirE1–VirE2 the protein bound predominantly to the poly-T ssDNA (Figure 6B). Dissociation was very slow in 100 mM NaCl buffer originally. Following exchange for 900 mM salt buffer, protein adsorption was reduced somewhat, but remained stably bound on the measurement time scale. Assays were then repeated for both ini-

tial adsorption and desorption at elevated salt and selected protein concentrations. Figure 6C and D show changes in % reflectivity as a function of time as protein was passed over the poly T (40 mer) DNA surfaces in a buffer containing 500 mM NaCl. As seen, at the high salt concentration VirE2 bound to poly-T rapidly but also dissociated rapidly, unlike in lower salt (Figure 6C). By contrast, VirE1–VirE2 binding (Figure 6D) was very similar to the behavior seen at low salt, in particular the very slow dissociation. Binding to poly-A (40mer) DNA was negligible for both VirE2 and VirE1–VirE2 as seen in Figure 2. We interpret these results to indicate that VirE2 binding to poly-T ssDNA is primarily electrostatic while binding of VirE1–VirE2 is not.

A model for VirE2 and VirE1–VirE2 binding to ssDNA

Based on insights from the present observations we propose the following interaction model for VirE2 with DNA. VirE2 alone exists in solution as filamentous aggregates. These are able to incorporate both short and long ssDNA substrates, converting from the disordered form to the ordered solenoidal capsid form as seen by electron microscopy (10,18,17). Long complexes are formed on both short and long ssDNA due to cooperative protein–protein interactions. These are mediated by both N to C terminal head-to-tail interactions and longitudinal links between each N terminal domain and the corresponding domain one turn around the solenoid (18).

The linear dependence of adsorption signal with protein concentration as seen in Figure 5C appears at odds with the well-known cooperativity of the VirE2-ssDNA interaction. One would rather expect a threshold below which very little binding occurs. However, when short ssDNA is bound to the surface it cannot be accommodated into an extended solenoid. Moreover the ssDNA substrates were too short to form a whole turn around the solenoid, whereas ring-to-ring contacts appear to provide the structural basis for cooperativity (18). Isolating these geometrical factors was the justification for the surface-based assay. What the simple cooperative binding paradigm misses, in this case, is that the VirE2 protein source in solution has *a priori* the form of filamentous aggregates. We consider that the SPRi signal reflects an anchoring of such aggregates at the surface, most likely at discrete points. Increasing concentrations of VirE2 in solution lead to an increase in total measured adsorption, which may reflect the equilibrium size distribution of soluble VirE2 filament lengths as well as the fraction of occupied DNA sites on the surface. ssDNA binding of VirE2 is suppressed at high ionic strength, consistent with a primarily electrostatic mode of interaction. This mode of VirE2 binding to ssDNA is highly sensitive to substrate flexibility as seen by the difference between short poly-T and poly-A sequences. Poly-T loops display purely entropic rigidity during conformational changes consistent with the standard worm-like chain model and persistence length of the order of 1 nm (26), whereas poly-A loops resist conformational change due to an additional 0.5 kcal mol^{-1} required for separation of each A–A pair (25). This suggests that while VirE2 forms a protective capsid on the T-strand without sequence specificity, the initial seeds of the interaction may well form preferentially at flexible locations. The strong cooperativity in protein–protein binding would then promote assembly of the solenoid structure even across the less flexible sites where binding of single protein units is unfavored.

We found that surface-bound ssDNA also interacts with heterodimeric VirE1–VirE2. In contrast to VirE2 alone, dissociation of VirE1–VirE2 from ssDNA is not accelerated at high salt. This points to a distinct mechanism of binding from that of VirE2, likely hydrophobic in origin. Since the acidic VirE1 hides the major positively charged DNA-binding face of VirE2, it is possible that VirE1–VirE2 interacts with ssDNA at a secondary binding site that is buried between protein units in the solenoidal complex. We can speculate that binding occurs at the intrinsically disordered N terminus that did not appear in the crystal structure of the VirE1–VirE2 complex. In common with VirE2, VirE1–VirE2 binds only weakly to the surface-bound strands of poly-A ssDNA and shows no binding to dsDNA. Therefore this secondary binding mode also requires substrate flexibility. At the highest concentrations of VirE1–VirE2, approaching 1 μM, a steep increase in the SPRi signal was observed (Figure 5C). This recalls a bulk condensation in the BET binding paradigm. Since in the absence of DNA the heterodimer remains fully soluble at this concentration, and since the SPRi signal is actually larger than that of VirE2 at lower concentrations, we may consider that the surface-bound DNA catalyses the growth of higher-order structures of VirE2.

As discussed in the introduction, the weight of existing evidence supports an independent transfer of VirE2 and the T-strand to the plant host. Specifically, complementation assays in which transformation is effected by mixed infection with one strain lacking T-DNA and a second lacking VirE2, show that their interaction is not essential in the bacterium (11). Also VirE2 antibodies did not pull down the T-strand in the 'TrIP' assay (13), and activation of the membrane-spanning VirB10 channel requires interaction with T-strand, but not VirE2, suggesting possibly a separate secretion pathway (27). While self-consistent, the evidence against an interaction remains indirect. Therefore we may consider two possibilities that are not, in fact, mutually exclusive. First, upon activation the concentration of VirE1–VirE2 within the bacterium during delivery of the T-strand to the type IV conjugative secretion system may not be altogether different from those of the present *in vitro* experiment. Then the secondary, non-electrostatic binding mechanism may seed the T-strand during its transit through the secretion channel. VirE1, lacking a secretion signal, is probably removed within the channel or at its entrance. While it is unlikely that a mature T-complex would pass the channel intact, a partially pre-seeded T-strand could be covered by VirE2 more rapidly and effectively than an entirely bare one. In the alternative case of bare and independent secretion, the T-strand must interact with VirE2 in its poorly soluble, filamentous aggregate form. The question arises how a long oligonucleotide can be rapidly covered by VirE2 protein. The present results suggest that even interactions with the oligonucleotide at the level of one or two VirE2 binding footprints are sufficient to capture a much larger aggregate. The T-strand is then rapidly covered by its protective capsid in the host cytoplasm without having to establish a binding equilibrium. Such a mechanism will not protect ev-

ery strand in the sense that some may not meet the VirE2 filaments at all, but every strand that is protected will tend to receive full coverage by the VirE2 capsid.

ACKNOWLEDGEMENTS

The authors are grateful to Drs Yoav Barak and Shira Albeck for training and support in protein purification, and to Peter Christie for feedback on the manuscript.

FUNDING

'Laboratoire Européen Associé' NaBi between the CNRS and the Weizmann Institute of Science; European Research Commission (TRACTAR project); Gerhardt M.J. Schmidt Center for Supramolecular Architecture. Electron microscopy was performed at the Irving and Cherna Moscowitz Center for Nano and Bio- Nano Imaging of the Weizmann Institute of Science. The Weizmann lab has benefited from the historical generosity of the Harold Perlman family. Funding for open access charge: European Research Commission (TRACTAR project).
Conflict of interest statement. None declared.

REFERENCES

1. Duckely,M. and Hohn,B. (2003) The VirE2 protein of Agrobacterium tumefaciens: the Yin and Yang of T-DNA transfer. *FEMS Microbiol. Lett.*, **223**, 1–6.
2. Gelvin,S.B. (2012) Traversing the Cell: Agrobacterium T-DNA's Journey to the Host Genome. *Front. Plant Sci.*, **3**, 52.
3. Gelvin,S.B. (2003) Agrobacterium-mediated plant transformation: the biology behind the 'gene-jockeying' tool. *Microbiol. Mol. Biol. Rev.*, **67**, 16–37.
4. Bhatty,M., Laverde Gomez,J.A. and Christie,P.J. (2013) The expanding bacterial type IV secretion lexicon. *Res. Microbiol.*, **164**, 620–639.
5. Christie,P.J. (2004) Type IV secretion: the Agrobacterium VirB/D4 and related conjugation systems. *Biochim. Biophys. Acta*, **1694**, 219–234.
6. Citovsky,V., Wong,M.L. and Zambryski,P. (1989) Cooperative interaction of Agrobacterium VirE2 protein with single-stranded DNA: implications for the T-DNA transfer process. *Proc. Natl. Acad. Sci. USA*, **86**, 1193–1197.
7. Christie,P.J., Ward,J.E., Winans,S.C. and Nester,E.W. (1988) The Agrobacterium tumefaciens virE2 gene product is a single-stranded-DNA-binding protein that associates with T-DNA. *J. Bacteriol.*, **170**, 2659–2667.
8. Sen,P., Pazour,G.J., Anderson,D. and Das,A. (1989) Cooperative binding of Agrobacterium tumefaciens VirE2 protein to single-stranded DNA. *J. Bacteriol.*, **171**, 2573–2580.
9. Deng,W., Chen,L., Peng,W.T., Liang,X., Sekiguchi,S., Gordon,M.P., Comai,L. and Nester,E.W. (1999) VirE1 is a specific molecular chaperone for the exported single-stranded-DNA-binding protein VirE2 in Agrobacterium. *Mol. Microbiol.*, **31**, 1795–1807.
10. Frenkiel-Krispin,D., Wolf,S.G., Albeck,S., Unger,T., Peleg,Y., Jacobovitch,J., Michael,Y., Daube,S., Sharon,M., Robinson,C.V. *et al.* (2007) Plant transformation by Agrobacterium tumefaciens: modulation of single-stranded DNA-VirE2 complex assembly by VirE1. *J. Biol. Chem.*, **282**, 3458–3464.
11. Otten,L., Greve,H.D., Leemans,J., Hain,R., Hooykaas,P. and Schell,J. (1984) Restoration of virulence of Vir region mutants of Agrobacterium tumefaciens strain B6S3 by coinfection with normal and mutant Agrobacterium strains. *Mol. Gen. Genet. MGG*, **195**, 159–163.
12. Citovsky,V., Zupan,J., Warnick,D. and Zambryski,P. (1992) Nuclear localization of Agrobacterium VirE2 protein in plant cells. *Science*, **256**, 1802–1805.
13. Cascales,E. and Christie,P.J. (2004) Definition of a bacterial type IV secretion pathway for a DNA substrate. *Science*, **304**, 1170–1173.
14. Engström,P., Zambryski,P., Van Montagu,M. and Stachel,S. (1987) Characterization of Agrobacterium tumefaciens virulence proteins induced by the plant factor acetosyringone. *J. Mol. Biol.*, **197**, 635–645.
15. Citovsky,V., DE Vos,G. and Zambryski,P. (1988) Single-Stranded DNA Binding Protein Encoded by the virE Locus of Agrobacterium tumefaciens. *Science*, **240**, 501–504.
16. Citovsky,V., Guralnick,B., Simon,M.N. and Wall,J.S. (1997) The molecular structure of agrobacterium VirE2-single stranded DNA complexes involved in nuclear import. *J. Mol. Biol.*, **271**, 718–727.
17. Abu-Arish,A. (2004) Three-dimensional Reconstruction of Agrobacterium VirE2 Protein with Single-stranded DNA. *J. Biol. Chem.*, **279**, 25359–25363.
18. Bharat,T.A.M., Zbaida,D., Eisenstein,M., Frankenstein,Z., Mehlman,T., Weiner,L., Sorzano,C.O.S., Barak,Y., Albeck,S., Briggs,J.A.G. *et al.* (2013) Variable internal flexibility characterizes the helical capsid formed by agrobacterium VirE2 protein on single-stranded DNA. *Structure*, **21**, 1158–1167.
19. Dym,O., Albeck,S., Unger,T., Jacobovitch,J., Branzburg,A., Michael,Y., Frenkiel-Krispin,D., Wolf,S.G. and Elbaum,M. (2008) Crystal structure of the Agrobacterium virulence complex VirE1-VirE2 reveals a flexible protein that can accommodate different partners. *Proc. Natl. Acad. Sci. USA*, **105**, 11170–11175.
20. Simone,M., McCullen,C.A., Stahl,L.E. and Binns,A.N. (2001) The carboxy-terminus of VirE2 from Agrobacterium tumefaciens is required for its transport to host cells by the virB-encoded type IV transport system. *Mol. Microbiol.*, **41**, 1283–1293.
21. Duckely,M., Oomen,C., Axthelm,F., Van Gelder,P., Waksman,G. and Engel,A. (2005) The VirE1VirE2 complex of Agrobacterium tumefaciens interacts with single-stranded DNA and forms channels. *Mol. Microbiol.*, **58**, 1130–1142.
22. Bouffartigues,E., Leh,H., Anger-Leroy,M., Rimsky,S. and Buckle,M. (2007) Rapid coupling of Surface Plasmon Resonance (SPR and SPRi) and ProteinChip^{TM} based mass spectrometry for the identification of proteins in nucleoprotein interactions. *Nucleic Acids Res.*, **35**, e39.
23. Nogues,C., Leh,H., Lautru,J., Delelis,O. and Buckle,M. (2012) Efficient antifouling surface for quantitative surface plasmon resonance based biosensor analysis. *PLoS ONE*, **7**, e44287.
24. Citovsky,V., DE Vos,G. and Zambryski,P. (1988) Single-Stranded DNA Binding Protein Encoded by the virE Locus of Agrobacterium tumefaciens. *Science*, **240**, 501–504.
25. Goddard,N.L., Bonnet,G., Krichevsky,O. and Libchaber,A. (2000) Sequence dependent rigidity of single stranded DNA. *Phys. Rev. Lett.*, **85**, 2400–2403.
26. Chen,H., Meisburger,S.P., Pabit,S.A., Sutton,J.L., Webb,W.W. and Pollack,L. (2012) Ionic strength-dependent persistence lengths of single-stranded RNA and DNA. *Proc. Natl. Acad. Sci.*, **109**, 799–804.
27. Cascales,E., Atmakuri,K., Sarkar,M.K. and Christie,P.J. (2013) DNA Substrate-Induced Activation of the Agrobacterium VirB/VirD4 Type IV Secretion System. *J. Bacteriol.*, **195**, 2691–2704.